Frontiers in Scientific Research and Technology

Online ISSN: 2682-297
Print ISSN: 2682-2962
http://fsrt.journals.ekb.eg

FSRT J 5 (2023) 41 - 51 10.21608/FSRT.2022.177796.1076

Synthesize Structural, Dielectric, and Optical Properties of Phosphorus Pentasulfide Modified Co-Polyurethane for Electrical Applications

F. A. Ibrahim[1,*], Magd M. Badr[2]

[1] Department of Physics, Faculty of Science, Al-Arish University, Al- Arish,45511, Egypt.

[2] Polymer Laboratory, Petrochemical Department, Egyptian Petroleum Research Institute, Cairo, 11727, Egypt.

ARTICLE INFO

Article history:
Received 16 December 2022
Received in revised form 29 December 2022
Accepted 31 December 2022
Available online 7 January 2023

Keywords
Co-polyurethan,
Structure properties,
Dielectric properties,
Optical properties.

ABSTRACT

A novel composition of co-polyurethane modified phosphorus pentasulfide is formed. The formed polyurethan is the source of N and O elements in the formulation, while phosphorus pentasulfide is the source of P and S. A rich P, S, N, and O element polymeric material of co-polyurethane is synthesized. The isocyanate part is toluene diisocyanate, and the polyol part is a mixture of novolac phenol formaldehyde resin and polyethylene glycol 600. Fourier-transform infrared spectroscopy (FT-IR), X-ray diffraction (XRD), and thermal analysis of differential scanning calorimetry (DSC) elemental analysis are used to characterize the synthesized materials. Phosphorus, sulfur, nitrogen, and oxygen elements are electron donor negative charged elements that have free pairs of electrons which are able to share in the molecule resonance and conjugation, increasing the optical, electrical, and other desired properties. The energy gaps computed for direct and indirect transitions were 2.25 and 2.205 eV, respectively. With modified phosphorus pentasulfide, the optical energy gap value and band energy tails decrease (PPS). The electrical conductivity of the composites at various temperatures was found to be similar to that of semiconducting materials, and the activation energy was calculated. They may therefore be interesting materials for electrical applications.

1. Introduction

In recent years, some research responsibilities for the synthesis of polymeric materials with donor groups have been mentioned. By boosting the electron resonance and free electron pairs, the targeted donor groups that contain phosphorus, sulfur, nitrogen, and oxygen may be differentiated. It was anticipated that the donor group would produce many of the desired features of the material. These characteristics of the generated polymeric material enable it to be used in a variety of applications. Flame retardant, supercapacitor, superconductor, semiconductor, catalyst, sensor, metal extraction, metal uptake, and battery are only a few of these uses [1-16]. Copolyesters for poly(butylene succinate) containing phosphorus were created, studied, and used as flame retardants. It was discovered that adding phosphorus-containing compounds to resin for modification boosted the flame retardant [1], and polyurethane ionomers with phosphate groups were synthesized and characterized [2]. In the current research, phosphorus pentasulfide (PPS) was used as a reactant to create a new co-polyurethane (PU/PPS) that contains both phosphorus and sulfur.

Numerous organic materials contain both nitrogen and oxygen atoms in their chemical makeup, but fewer organic products contain phosphorus and sulfur, and it is uncommon for all four of those elements—P, S, N, and O—to be present. To create a co-polyurethane material with unique features, phosphorus pentasulfide and polyurethane serve as the sources of P and S, nitrogen, and oxygen, respectively. The aim is to synthesize and use various analytical techniques to investigate the structure, optical, and dielectric characteristics of phosphorus pentasulfide modified Co-Polyurethane (PU/PPS).

2. Experimental Technique

2.1 Raw Materials

In the current investigation, the following chemicals were used: The SPREA MISR Company, 10th Ramadan Industrial City, Cairo, Egypt, provided the novolac phenol formaldehyde resin (NOV) in granular powder form. Egypt's Adwic - El Nasr Pharmaceutical Co. contributed the phosphorus pentasulfide (PPS), polyethylene glycol 600 (PEG-600), toluene diisocyanate (TDI), and methyl ethyl ketone (MEK). Without any additional purification, analytical grades of all components, including solvents, have been employed. The synthesis of PU/PPS and the use and handling of phosphorus pentasulfide both adhered to all safety considerations and guidelines.

* Corresponding author at Al-Arish University

E-mail addresses: fahmed_ibrahim@yahoo.com (F.A. Ibrahim)

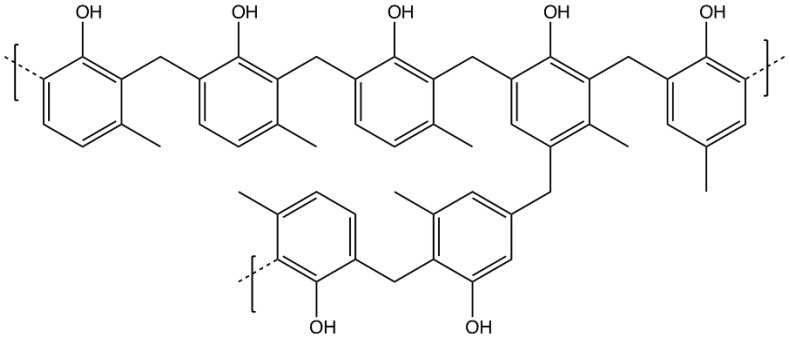

Novolac phenol formaldehyde resin (NOV)

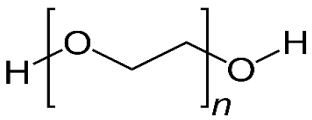

Polyethylene glycol (PEG-600)

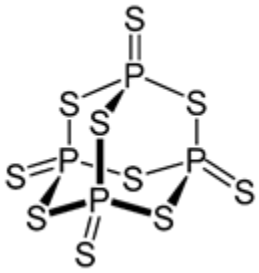

Phosphorus pentasulfide (PPS)

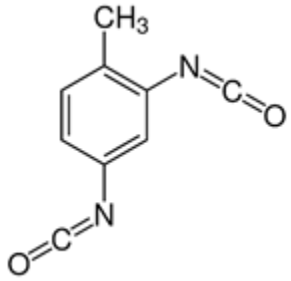

Toluene diisocyanate (TDI)

2.2. Synthesis process and film formation

10 g of novolac phenol formaldehyde resin (NOV) was dissolved in 10 ml of methyl ethyl ketone (MEK), and 5 g of phosphorus pentasulfide (PPS) was added to the mixture dropwise. At room temperature, the mixture was stirred for 10 minutes. A totally clear solution was created by adding 20 ml of toluene diisocyanate (TDI) hardener drop by drop while stirring continuously for 30 min at room temperature. The created sample is designated with the letters (PU/PPS). The Doctor blade technique was used to create thin films on glass substrates for dielectric and optical measurements, while the remaining material was cast in petri dishes for FT-IR, XRD, and thermal analysis of DSC characterization and analysis. The prepared samples were oven-cured overnight at 80 ^{o}C before being kept at room temperature for 24 hours before being measured. All safety and hazard requirements were observed at every stage of the synthesis process, according to the material safety data sheet (MSDS) for PPS.

2.3. Characterization and Properties

The structure of the synthesized materials was analyzed using powder X-ray diffraction (XRD) analysis. A PHILIPS X'Pert diffractometer with a Cu K target, Ni filter, and 40 kV and 30 mA tube tension was used for the XRD investigation. Diffractograms were taken in the 2θ range between 4o and 80o for X-ray radiation source (λ= 1.5406 Å) powered. The functional groups of the reactant ingredients are investigated by using Fourier transformation - Infrared (FT-IR) profiles. Differential scanning calorimetry (DSC) thermogram with Detector Type: DSC-60, Detector Serial No:C30454400673SA was used to examine the sample's thermal stability, Atmosphere: Nitrogen, Gas Flow: 20[ml/min], Pan Name:

Aluminum Seal, Sample Weight: 2.000 [mg], Temp. Rate: 10.00 [C/min], Hold Temperature: 100.0 [C], Hold Time: 0[min]. An RLC analyzer (Model 1061, Chen Hwa, LCZ METER, CHINA) was used to test the dielectric characteristics (dielectric constant/loss) of the thin film sample from 40Hz to 200 kHz at room temperature. A multimeter Keithley 760 was used to obtain the dc data, hence, the I–V characteristic between electrodes was calculated. The DC conductivity (σ) of the prepared film was measured at temperatures ranging between 300 and 400 K using silver paste electrodes (two probe methods). The optical properties of synthesized samples were investigated using a spectrophotometer. A spectrophotometer of type Jasco-870 (Instruments, England) was used to expose the produced film to ultraviolet (UV) light. In the wavelength range of 90-2500 nm, the optical absorbance and transmittance spectra of the film were obtained at room temperature. During the absorption process, a known energy photon stimulates an electron from a lower energy state to a higher energy level.

3. Results and discussion

3.1. IR Spectra

Different types of bonding are anticipated to form depending on the number of functional groups present in the reactant elements. This may possibly be because the formulation of the created polymeric composite material contains polar atoms of phosphorus, sulfur, nitrogen, and oxygen. Figure 1 and Table 1 show the FT-IR spectra and the spectra data of the produced composite resin sample.

The P=medium-intensity S's stretching vibration band is located at 760 cm^{-1}. It's possible that the P-S bond stretching vibration, which was caused by the proximity of strong electronegativity groups and atoms, caused the band of varying intensity to appear at 555 cm^{-1}. Pentavalent and trivalent methoxy compounds were discovered at 1086 cm^{-1} and 1182 cm^{-1} of the asymmetric stretching vibrations of the aliphatic methoxy P-O-C group, respectively, and at 1384 cm^{-1} of the recognizable symmetric methyl deformation band. At 951 cm^{-1}, pentavalent ethoxy compounds also showed a prominent band. A prominent band at 827 cm^{-1} is present in methoxy and ethoxy compounds, which is most likely the result of the P-O-C group being stretched symmetrically. A sharp band at 1182 cm^{-1} is caused by the P-O-C methoxy group. The strong band at 951 cm^{-1} combines with the band caused by the P-O-C asymmetric stretching vibration for aromatic compounds, P-O-phenyl. In the range of 795-650 cm^{-1}, the P-C bond's stretching vibration produces a medium-to-strong band. The medium-to-strong intensity band of the phenyl-P bond is caused by an aromatic ring vibration that takes place at 1455 cm^{-1} and is of. In the range of 1350-1150 cm^{-1}, the P=O group's strong stretching vibration band is seen. It is possible that all of the phosphorus atoms were involved in other types of bonding as a result of the absence of the sharp band of the P-H group stretching vibration at the regions of 2265-2285 cm^{-1} and the absence of the weak-to-medium intensity broad bands of the P-O-H group of its O-H stretching vibration at 2100-2300 cm^{-1} and its hydrogen bonding at 2560-2700 cm^{-1}. The carbonyl stretching vibration of the amide of urethanes, which occurs in the range of 1725 cm^{-1}, is also visible in the bands of the urethane group. Due to the N-H stretching vibration, primary urethane exhibits a variety of absorptions in the range of 3450-3200 cm^{-1}. At near 3300 cm^{-1}, secondary urethane hydrogen bonds are absorbed. Due to the NH_2 group's deformation vibrations, primary urethanes exhibit a medium-to-strong band at 1606.26 cm^{-1}. The CHN group vibration causes associated secondary urethanes to absorb substantially in the vicinity of 1510 cm^{-1} [17-18].

3.2. X-Ray Diffraction

The polymeric blend material of NDTE treated with PPS was investigated for phase purity and crystallinity using the X-ray diffraction technique, as shown in Figure 2. (XRD). With the information provided above, a broad peak was seen at 2Theta = 19.88° on the X-ray diffraction angles, showing that the created material has a fine structure or partially crystalline phase and the crystalline structure of the resin has not altered since PPS was added. The synthesized material only has one phase, which shows that a chemical reaction took place. The explanation for the less pure phase is being clarified by the noisy chart; this may be because several active atoms and functional groups were obtained. We concluded that adding PPS material did not affect the crystalline behavior. [19–22].

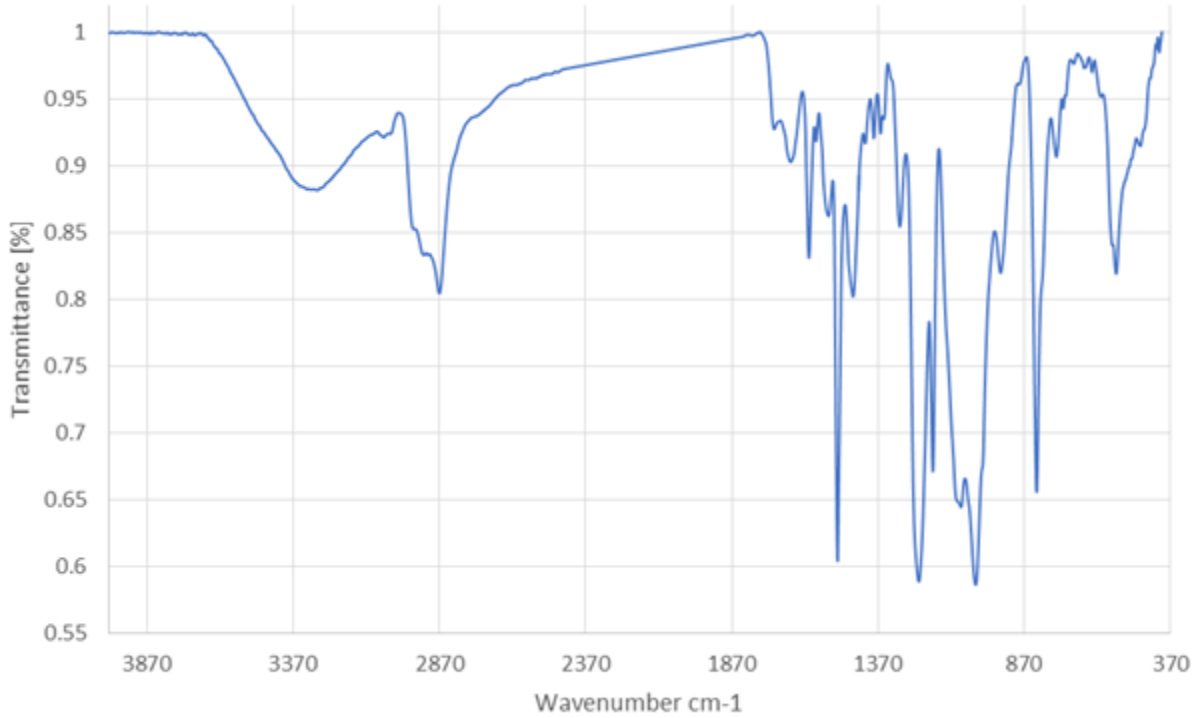

Fig. (1) FTIR Spectra of the Prepared Polyurethan/Novoalc/Phosphorus pentasulfide Composite (NEUPC).

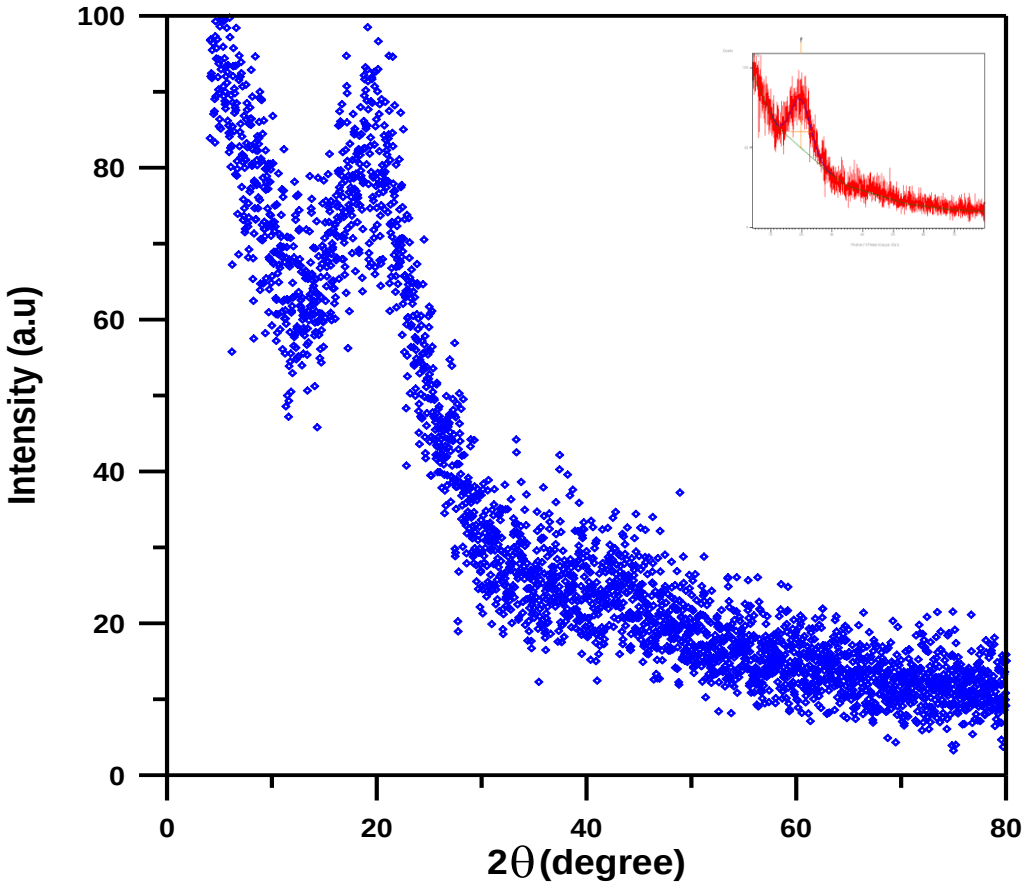

Fig. (2) XRD pattern of the Prepared Polyurethan/Novoalc/Phosphorus pentasulfide Composite (NEUPC)

Peak List

Pos.[°2Th.]	Height [cts]	FWHMLeft[°2Th.]	d-spacing [Å]	Rel. Int. [%]
19.88(8)	20(1)	7.4(2)	4.46282	100.00

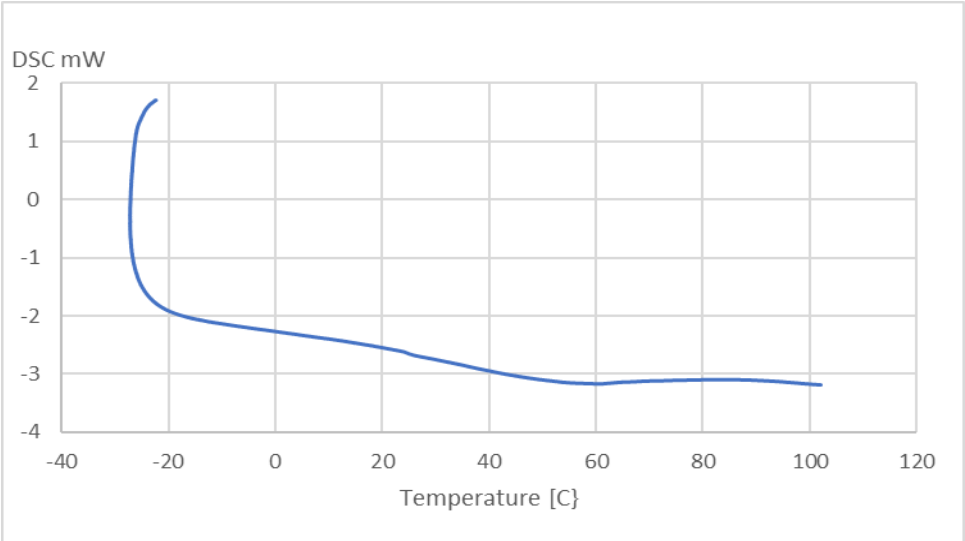

Fig. (3) DSC thermogram of the Prepared Polyurethan/Novoalc/Phosphorus pentasulfide Composite (NEUPC).

3.3. (DSC) Differential Scanning calorimetry

The thermogram of the Prepared Polyurethan/Novoalc/Phosphorus pentasulfide Composite (NEUPC) from differential scanning calorimetry (DSC) is shown in Figure 3. It is demonstrated that every sample's viscosity and thermal stability are dependent on the temperature difference $\Delta T = T_c - T_g$ [23, 24]. On the other hand, these samples have demonstrated the difference ΔT and can be used to create a variety of shapes, including sheets and thin films. Evidently, research using differential scanning calorimetry (DSC) on numerous samples revealed that the coordination number of the network formerly affects how glass transforms (T_g). The glass transition temperature peaked at 56.18 °C, but it actually began at 24.27 °C and concluded at 77.24 °C with heat values of -48.45 mJ and -24.23 J/g, showing that the polymeric material had partially crystalline and a single phase composition before that temperature, which confirms results of X-Ray Diffraction [25–27].

3.4. Dielectric properties

Figures 4 and 5 depict the frequency dependence of the dielectric constant and dielectric loss at room temperature. The dielectric constant and dielectric loss of the sample under study decrease as frequency increases, which are related to the energy stored and dissipated, respectively. This phenomenon was caused by reductions in dielectric dispersion created by the non-polar polymer [28-30].

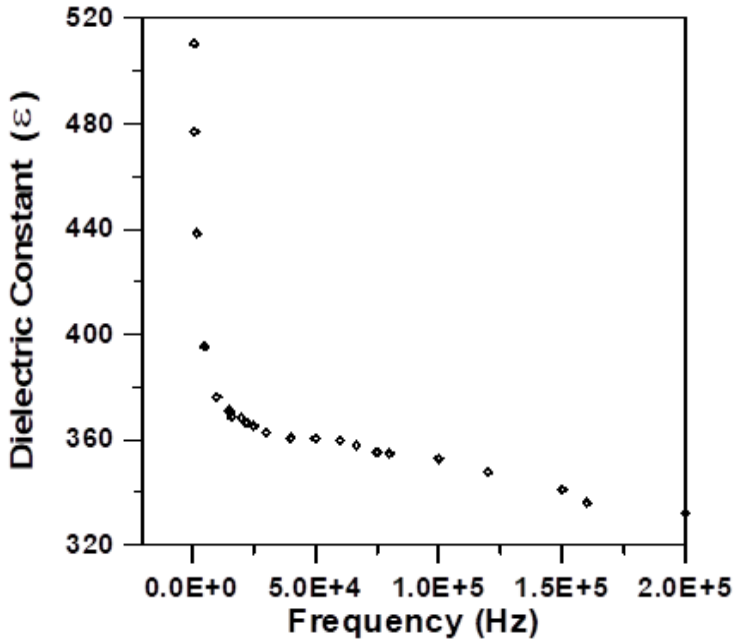

Fig. (4) Dependence of dielectric constant on frequency

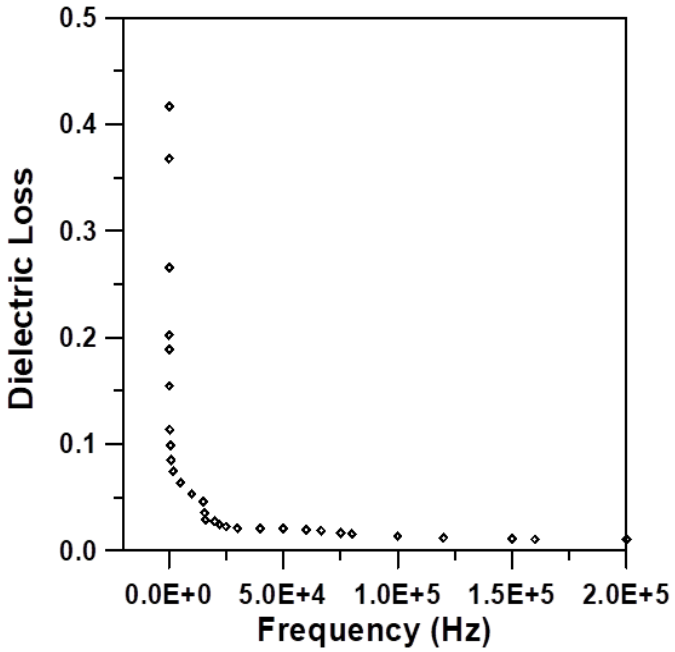

Fig. (5) Dependence of dielectric loss on frequency

At low frequencies, there are contributions from conductance and interfacial processes. At low frequencies, ions can travel great distances and may influence the dielectric constant [31,32]. As shown in Figure 4&5 the dielectric constant and dielectric loss seems to maintain nearly constant at high frequencies. According to a recent study [33-36], a polymer dielectric constant is primarily characterized by two factors. The first is the polarizability of molecules, which may be altered by modifying the kind and quantity of polarizable groups. Following that is the polymer's free volume.

Figure (6) depicts a conductivity measurement with frequency, illustrating that the conductivity dependency on frequency is linear. The conductivity was calculated from the following equation [37]:

$$\sigma = \sigma_0 + A\omega^n \quad \textbf{(1)}$$

where σ_0 is the conductivity to direct current (DC), $\omega = 2\pi f$, since f is the frequency, while A and n (which have values between 0 and 1) are parameters that depend on temperature and samples.

Equation (1) predicts distinct tendencies: one of them the conductivity (DC) term dominates at low frequencies and there is no dependency between conductivity and frequency, on the other hand, the conductivity (DC) has a potential reliance on the frequency at higher frequencies as dispersed behavior arises and in place of the DC behavior. As demonstrated in Fig.(6), conductivity is depicted in a direct current (DC) domain for low frequencies, whereas the AC current regime dominates for high frequencies and all composites [30]. Figure 6 shows the conductivity increases to a high value across a frequency range (40 Hz–200KHz).

The addition of phosphorus pentasulfide (PPS) inside the mixture results in a considerably more conductive polymer and is employed to increase the electrical conductivity of this composition [38-40]. The impedance reduced as frequency increased (Fig. 7), showing that the film sample grew more conductive.

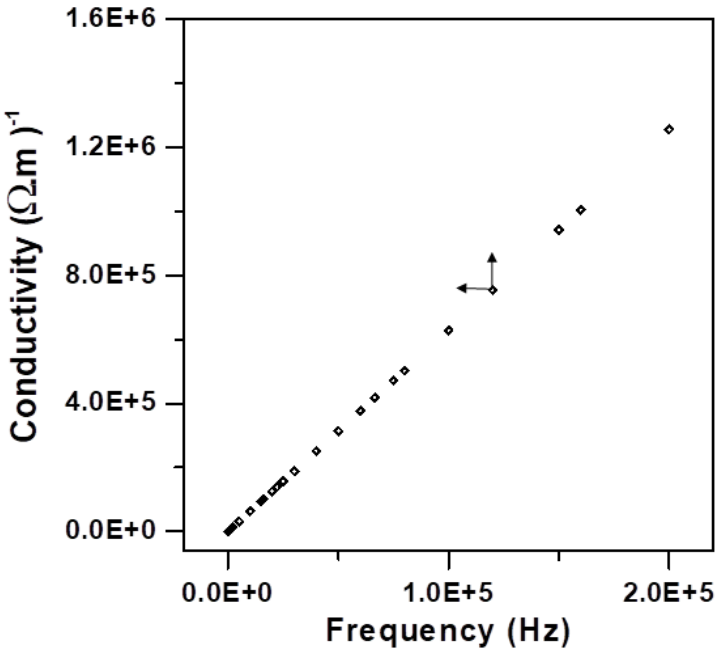

Fig. (6) The conductivity versus frequency measurement at room temperature

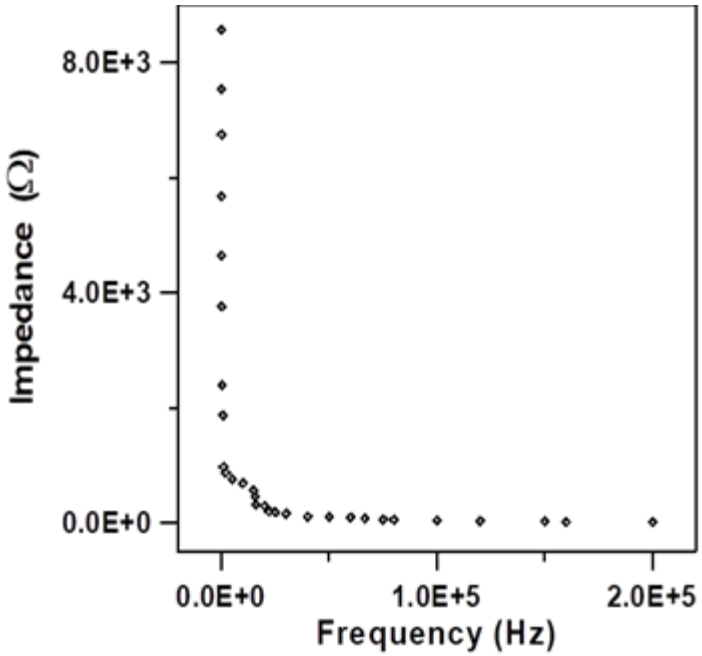

Fig. (7) Impedance versus frequency for film sample

Figure (8) illustrates the dc electrical conductivity of the prepared film sample measured at temperatures ranging from 300 to 400 K. The following equation [41] can be used to calculate conductivity:

$$\sigma = \sigma_0 \exp(-\Delta E/kT) \quad (2)$$

where σ is the conductivity, σ_0 is the pre-exponential factor, T is the material temperature in K, ΔE is the conduction activation energy, and k is the Boltzman constant. The conduction activation energy (ΔE) is defined as the smallest amount of energy necessary to initiate an electrical conduction chemical reaction. Straight lines could be fitted to the conductivity data, and the activation energy and pre-exponential factor were calculated. Conductivity changes significantly as temperature increases. The conductive mechanism of the temperature range is that the valence band is fully occupied and strongly separated from conduction, and the barrier between them prevents electrons from being activated for charge transfer. As a result, the temperature is insufficient to allow electrons to flow through the barrier. In the conduction and valence bands, the primary charge carriers are electrons and holes, respectively. The mobility (μ) and concentrations of holes and electrons, that quantify the transportation capacity of charge carriers in the composite, are regarded to be the basic parameters of these [42, 43]. The hopping mechanism transport charge is appropriate for synthetic polymers [44]; when two distinct charge carriers, such as holes and electrons, are separated by a potential barrier, one can transfer to the other via tunneling the barrier or crossing over the barrier through an active state [45]. Activation energy calculation revealed that it was small (= 0.51 ev), hence, the Dc conductivity increased.

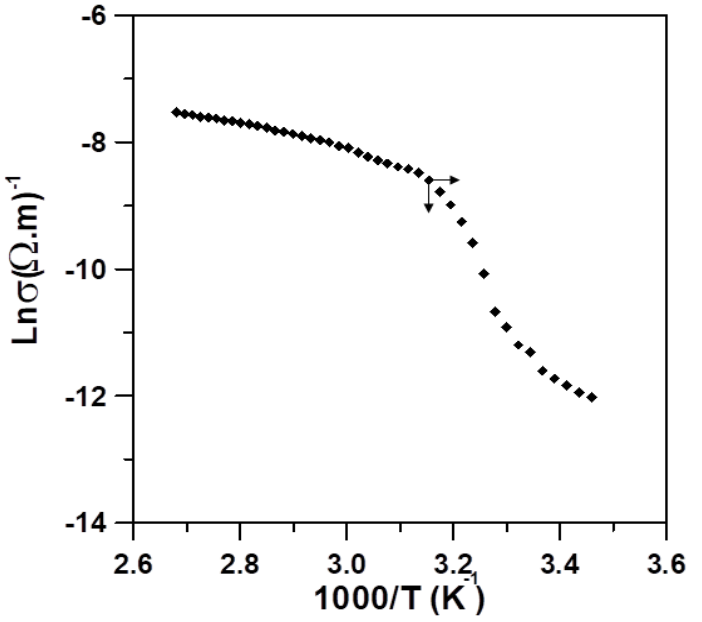

Fig. (8) The dependence of conductivity on temperature for film sample

Despite the fact that the ΔE parameter is evolving, the changes detected are significant. Figure 8 depicts the presence of two lineal regions in the DC conductivity vs 1/T plot. This indicates that crystalline structures stay in the temperature interval, and DC conductivity has been seen to rise progressively with temperatures up to 100 ^{o}C. The energy would be substantial enough to increase the free volume in the system due to high temperatures (i.e., 100 ^{o}C), allowing tiny particles to move more freely. The addition of PPS amounts increases the electrical properties

of the composite, this gives the possibility to use composite for high–requirement applications, such as industrial electrical applications. As a result of the analysis, the studied composite has acceptable levels of industrial electrical applications.

In conclusion, the use of PPS in composites can effectively raise the dielectric constant. At the same time, there is a negligible gain in electrical conductivity over pure composite. These effects are caused by the composite matrix's significant electrical polarization of PPS particles. Furthermore, the addition of PPS to the composite improved not only the dielectric characteristics of the film sample but also its electrical conductivity.

3.5 Optical properties

The absorption coefficient(α) as a function of photon energy, the reflectance (R), and the transmittance (T) as a function of wavelength are shown in figure (9). The optical reflectance and transmittance spectra for the polyurethane/novolac phenolic resin (PU/NOV) doped with Phosphorus pentasulfide (PPS) film in the (90–2500 nm) wavelength range are shown in Fig. 9. (a & b). The optical transmission measurements are used to determine a variety of parameters that may aid in developing a better understanding of the optical characteristics of the film sample.

The absorption coefficient (α) was calculated directly from the absorption spectra using Beer-Lambert law =2.303(A/d) [46], since (d) is the film thickness and (A) is the absorbance. The absorption coefficient (α) related to the incident photon's energy (hυ) (Fig.9.c) obeys the following equation [47, 48]:

$$\alpha(h\upsilon) = B(h\upsilon - E_{opt})^n \quad \textbf{(3)}$$

Where E_{opt} is the optical energy gap, B is a constant, and the exponent n is an index, that can be expected to have values of 1/2,3/2,2 and 3 determined by the type of electronic transition causing the optical absorption, n=2 for indirect allowed transition, n=3 for forbidden indirect transition, n=1/2 for allowed direct transition, and n=3/2 for forbidden direct transition. The indirect and direct energy gap is estimated by plot $(\alpha h\upsilon)^{1/2}$ and $(\alpha h\upsilon)^2$ as a function of photon energy (hυ) for the film as illustrated in Fig. (10).

Extrapolating the graphs' linear component (Fig. 10) to intersect the photon energy axis yields values E_d & E_{ind} that equal 2.25 ev for allowed direct transition and 2.205 ev for allowed indirect transition. The reduction in the optical energy gap caused by distributed PPS particles can be explained by the insertion of tiny quantities of conducting film samples, which generates charge transfer routes [49, 50]. The Urbach formula [51] describes the absorption coefficient (α) as the following:

$$\alpha(h\upsilon) = \alpha_o e^{h\upsilon/\Delta E} \quad \textbf{(4)}$$

where ΔE is the tail of the energy gap (the energy which is interpreted as the tail width of the localized state of the forbidden band gap) and α_o is a constant [52].

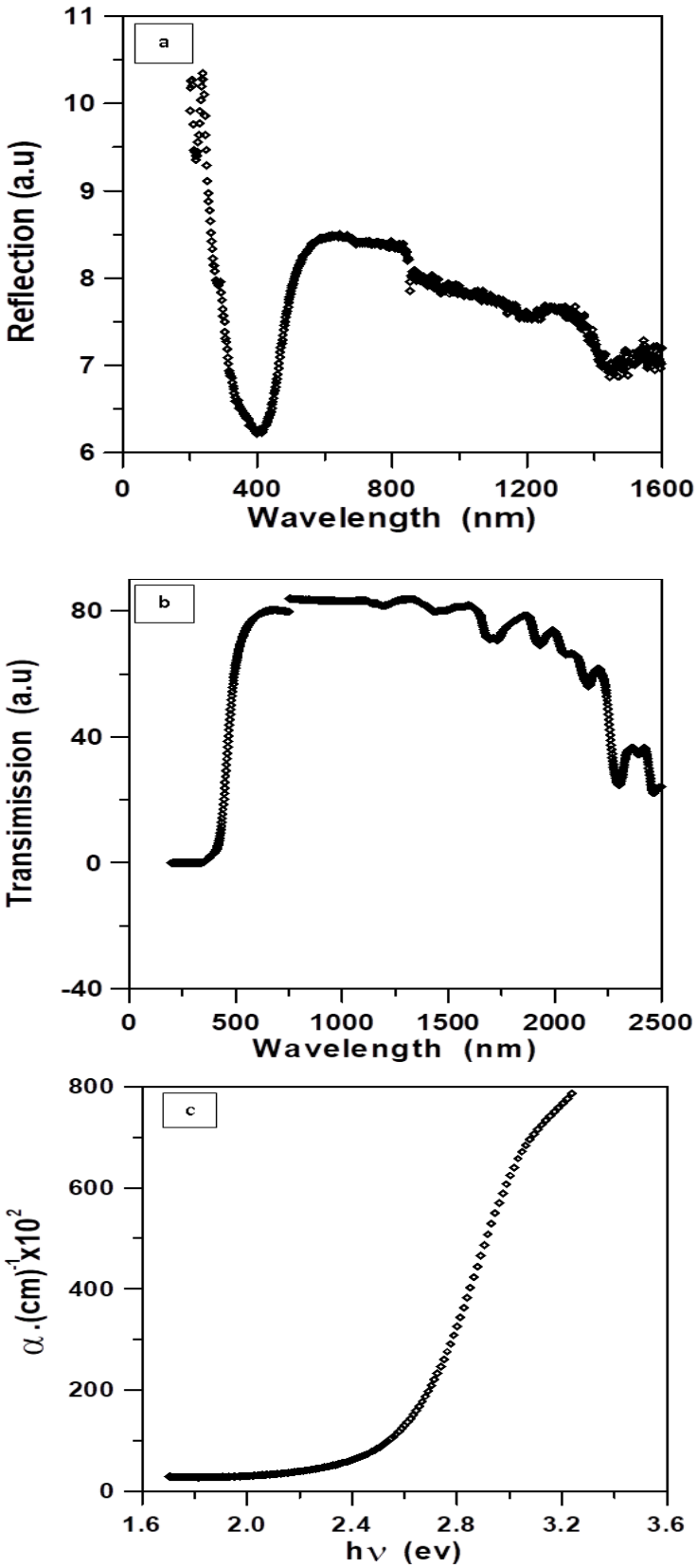

Fig. (9) The transmittance (T) **(a)**, the reflectance (R), **(b)** as a function of wavelength, and the absorption coefficient(α) as a function of photon energy, **(c)** for film sample.

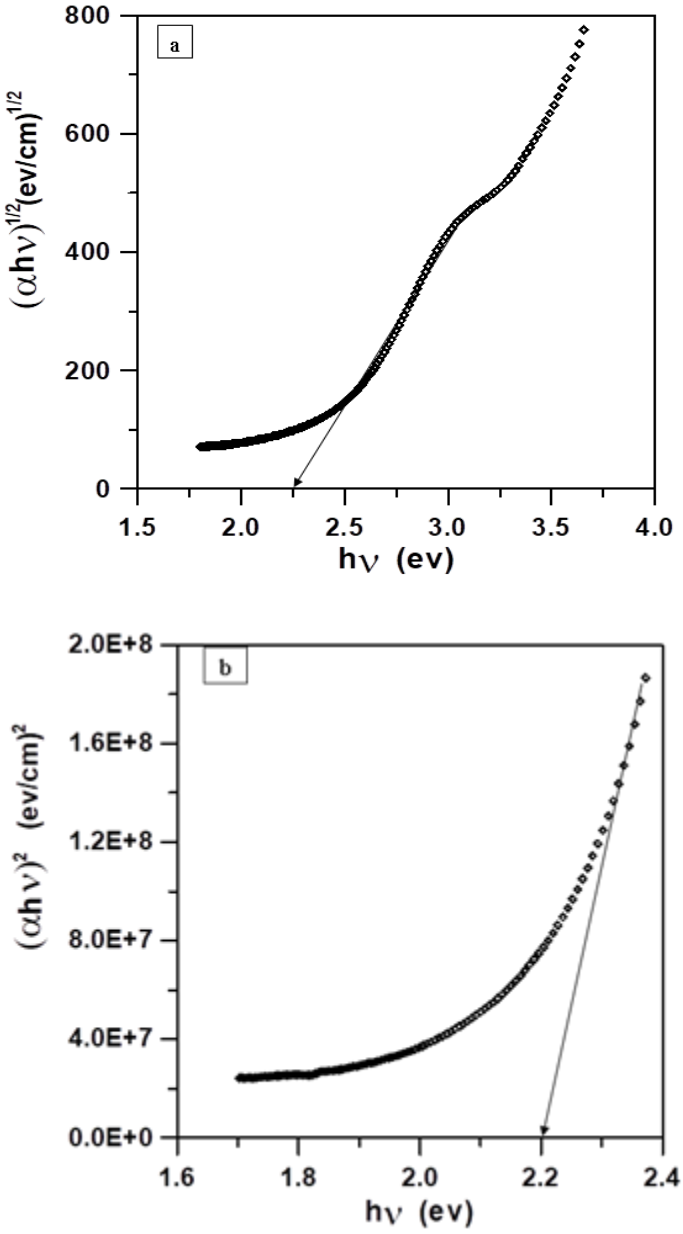

Fig. (10) (a) The allowed direct $(\alpha h\nu)^{1/2}$ and **(b)** indirect $(\alpha h\nu)^2$ transition as a function to photon energy (hν) for the film sample.

The breadth of the Urbach tail of the localized states due to defect levels in the transition gap was calculated using Equation (4) [52]. Figure 8 illustrates the linear dependency of ln(α) vs photon energy (hu). The size of the breadth of the band tail ΔE is given by the reciprocal of the slopes of the curve which was equal to 0.37 eV. The decrease in Urbach tail breadth caused by PPS might be attributed to the integration of conducting PPS into the polymer chain, which expands the density of states further into the visible area of the electromagnetic spectrum than in the PPS case [53]. The PPS energy tails have the smallest values due to the neatness of their structure and the scarcity of impurities, leading to a decrease in the localized states.

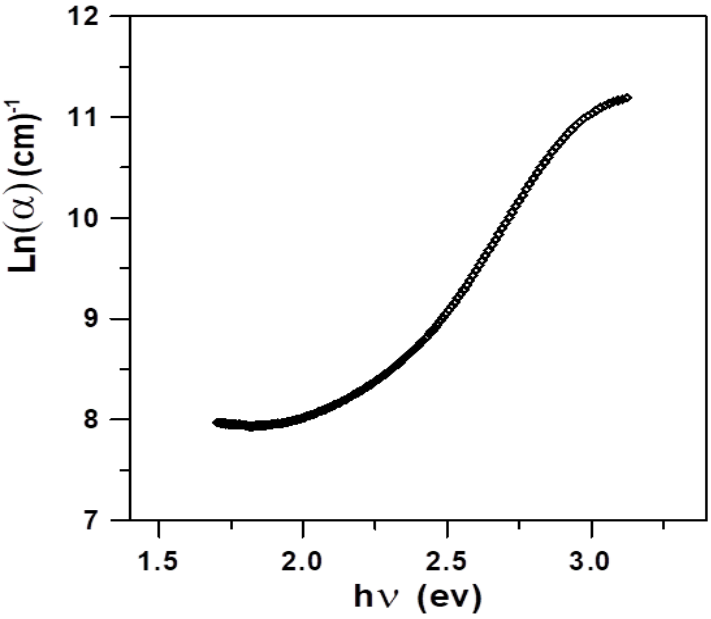

Fig. (11) Dependence of ln(α) versus photon energy (h υ) for film sample

The light reflectivity theory was utilized to derive the extinction coefficient (k) and the refractive index (n). The following equations were used to determine the values of k and n [54, 55].

$$k = \frac{\alpha\lambda}{4\pi} \quad (5)$$

And

$$n = \frac{\left(1+\sqrt{R}\right)}{\left(1-\sqrt{R}\right)} \quad (6)$$

Fig. 12 shows (b) extinction coefficient (k), and(a) Refractive index (n), as a function of wavelength. It demonstrates that the refractive index (n) drops fast at lower wavelengths and the extinction coefficient (k) rises as the wavelength increases. The electrical measurements show that the variations in optical characteristics are caused by the composite's improving conductive nature.

Figures (13&14) depict the fluctuation of the film sample's imaginary and real dielectric constants. The complex dielectric constant is a fundamental material property. The real component is linked with how much it slows the speed of light in the material, whereas the imaginary component is related to how a dielectric absorbs energy from an electric field due to dipole motion. The relationship was used to compute the dielectric constant's real and imaginary parts [55].

$$\varepsilon^* = \varepsilon_1 - i\varepsilon_2 \quad (7)$$

The imaginary part of the dielectric constant ε_2, which is a function of extinction coefficient (k) and refractive index (n), is estimated by using the equation [55]:

$$\varepsilon_2 = 2nk \quad \textbf{(8)}$$

while the real part of the dielectric constant, ε_1, is calculated from the following equation:

$$\varepsilon_1 = n^2 - k^2 \quad \textbf{(9)}$$

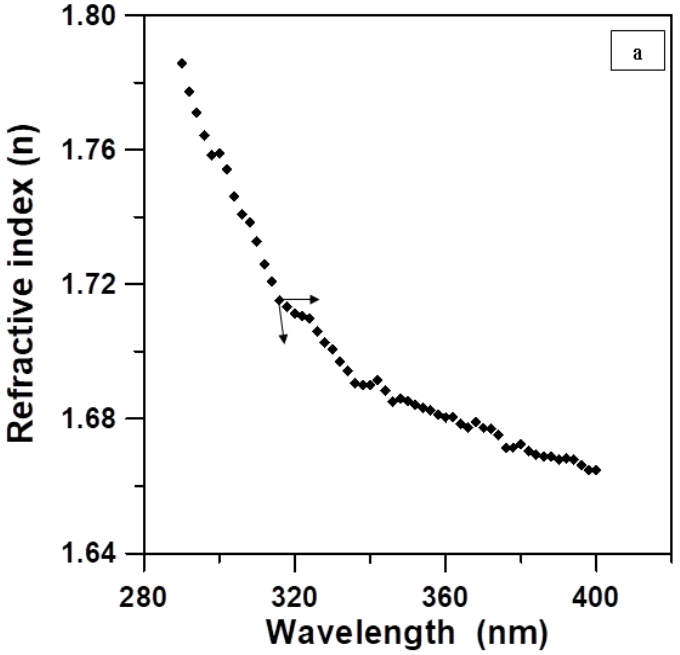

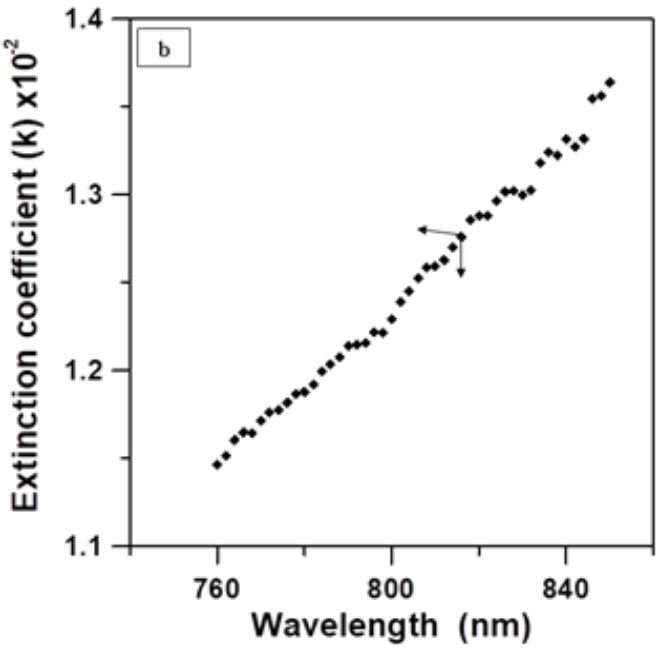

Fig. (12) (a) Refractive index (n), and **(b)** extinction coefficient (k), as a function of wavelength.

The real part of the dielectric constant, ε_1 grows progressively with photon energy, reaching its maximum value when the energy exceeds 3 eV, on the other hand, the imaginary part of the dielectric constant, ε_2 decreases progressively with photon energy, reaching its minimum value when the energy exceeds 3 eV. Furthermore, the real part is higher than the imaginary part dependent on the incident photon, indicating that the material responds to light more than its response to clear visuals [49].

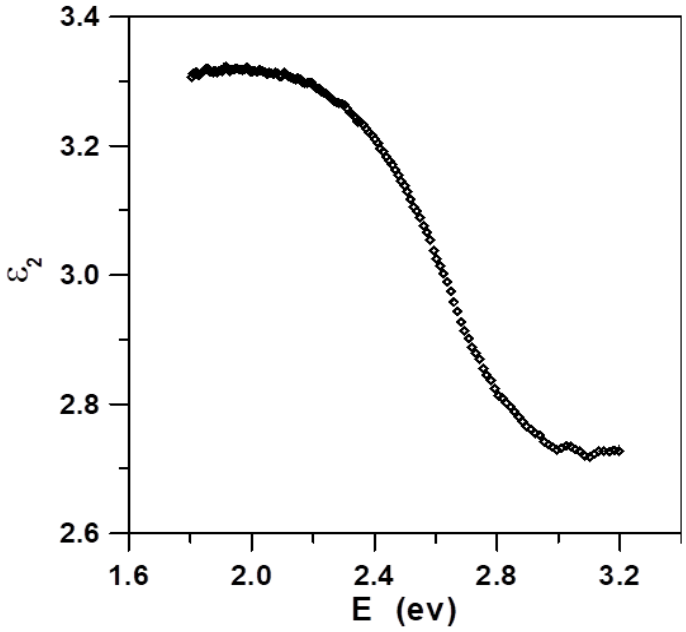

Fig. (13) Plot of imaginary part ε2 of the dielectric constant as a function of phonon energy for the film sample.

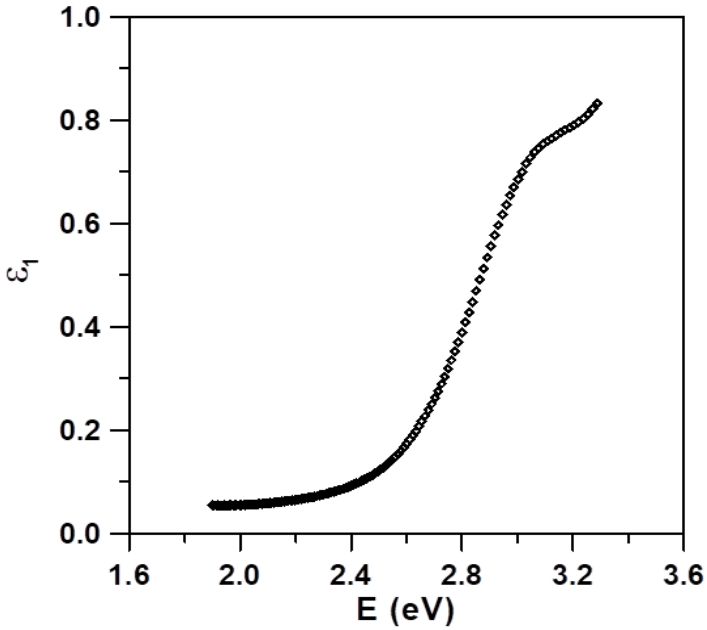

Fig. (14) Plot of real part ε_1 of the dielectric constant as a function of phonon energy for the film sample

Conclusion

In the current study, the XRD pattern and FT-IR profiles were employed to investigate the structure and interplanar d-spacing of the formed samples. The results of DSC are in agreement with XRD results. This work deals with the behavior of dielectric properties as a function of applied field frequency and the optical as a function of the wavelength of co-polyurethane-modified phosphorus pentasulfide. The optical characterization approach was used to study a film sample made by casting directly onto glass substrates with a doctor's blade. The transmittance spectrum in the visible regions was utilized to calculate optical characteristics such as extinction coefficient (k) and refractive index (n). where the energy gaps computed for direct and indirect transitions were 2.25 and 2.205 eV, respectively. The band energy tails and optical energy gap value decrease with modified phosphorus pentasulfide (PPS) compared to the same polymer without (PPS). The extinction coefficient increases as the wavelength increases, but the refractive index decreases as the photon wavelength rises. The bath surface volume energy loss function was produced using real and imaginary dielectric constant portions, and it has the greatest peak at energy region 3.2 eV, which leads to the single-electron excitation process that occurs in the film sample. According to the outcomes, the material had a new visual reaction to light, and the nature of the electrical transmission was indirect. When the energy range is 3.2 eV and the material possesses electrical conductivity and good visual properties, the dielectric value increases. Impedance decreases with increasing frequency. The dielectric loss and dielectric constant of the prepared film sample decrease with an increase in the applied frequency. The electrical conductivity of alternating current rises with frequency. The measured electrical conductivity of the composites is temperature dependent in a manner similar to that of semiconducting materials, and the activation energy was determined. In light of this, a novel composition of co-polyurethane-modified phosphorus pentasulfide might be intriguing material for electrical applications.

References

[1] Xiaoming Z., Tonghao W., Chemosphere 235 (2019) 163.
[2] Kakati D. K., George M. H., POLYMER, 34 (20) (1993) 4319
[3] https://bmcchem.biomedcentral.com/track/pdf/10.1186/1752-153X-6-132.pdf
[4] https://app.knovel.com/kn/resources/kpPBPFSA03/toc
[5]https://www.sciencedirect.com/science/article/pii/0079670093900269
[6]https://pubs.rsc.org/en/content/articlelanding/2014/ra/c4ra06080f
[7]https://www.mdpi.com/journal/polymers/special_issues/P_Polym
[8]https://onlinelibrary.wiley.com/doi/abs/10.1002/0471440264.pst237.pub3
[9] https://www.icevirtuallibrary.com/doi/10.1680/jgrma.16.00016
[10] https://www.amazon.com/Phosphorus-Based-Polymers-Synthesis-Applications-Chemistry/dp/1849736464
[11]https://www.degruyter.com/document/doi/10.1351/pac200779111879/html
[12] https://patents.google.com/patent/EP0376591A1/en
[13] https://pubs.acs.org/doi/10.1021/bm2004803
[14] http://www.eurekaselect.com/download_file
[15] https://www.nature.com/articles/natrevmats201755.pdf
[16]https://www.tandfonline.com/doi/epub/10.1080/14686996.2021.1908095? needAccess=true
[17] John Wiley & Sons Ltd, Baffins Lane, Chichester, “Infrared and Raman Characteristic Group Frequencies Tables and Charts”, Third Edition, New York, Published in 2001
[18] Hema M., Selvasekarapandian S., Arunkumar D., Sakunthala A., Nithya H., Journal of Non-Crystalline Solids 355 (2009) 84.
[19] Klop A., Lammers M., Polymer 39 (24) (1998) 5987.
[20] Huang, Tan K. S., Lin J., Tan K. L., Chemical Physics Letters 371 (2003) 80.
[21] Yang C. C., Materials Letters 58 (2003) 33.
[22] Motawie A. M., Mohamed M. Z., Ahmed S. M., El-Komy D., Badawy N. A., Abd El All A. Y., Sadak E. M., Russian Journal of Applied Chemistry, 88 (6) (2015) 970.
[23] Somdee P., Kuknyo T. L., Konya C., Szabo T., Marossy K., Journal of Thermal Analysis and Calorimetry volume 138 (2019) 1003.
[24] Tan C., Tirri T., Wilen C. E., Polymers, 9 (5) (2017) 184.
[25] Oprea S., J Polym Res 19 (2012) 9767
[26] Prisacariu C., Scortanu E., High Performance Polymers, (2011) 308.
[27] Stanzione M., Russo V., Oliviero M., Verdolotti L., Sorrentino A., Serio M. Di, Tesser R., Iannace S., Lavorgna M., Data in Brief 21 (2018) 269.
[28] Naskar A. K., Khastgir D., Bhowmick A. K., De, S. K. Effect of Chlorination of Ground Rubber Tire on its Compatibility with Poly (vinylchloride): Dielectric Studies. J.Appl. Polym. Sci. 84 (2002) 993.
[29] Genescà M. M., Amorós J. G., Rosas R. M., Massagués L., Colom X., Study and Characterization of the Dielectric Behavior of Low Linear Density Polyethylene Composites Mixed with Ground Tire Rubber Particles, Polymers 12 (2020) 1075.
[30] Saad A. L.G., Azi, H. A.;, Dimitry O. I. H. Studies of Electrical and Mechanical Properties of Poly(vinyl chloride) Mixed with Electrically Conductive Additives. J. Appl. Polym. Sci. 91 (2004) 1590.
[31] O’Neill R., Bowman M., Greg, J. M. Dielectric enhancement and Maxwell–Wagner effects in ferroelectric superlattice structures. Appl. Phys. Lett. 77 (2000) 1520.
[32] Petrovic´ M. M. V., Bobic´ J. D.,; Ramoška T.; Banys J., Stojanovic´ B. D., Antimony doping effect on barium titanate structure and electrical properties. Ceram. Int. 37 (2011) 2669.
[33] McCru, N. G.,; Read B. E., William, G., Anelastic and Dielectric Effects in Polymeric Solids; Dover Publications, INC.: New York, NY, USA, 1991
[34] Kalogeras I. M., Pallikari-Viras F., Vassilikou Dov, A., Dielectric and thermal characterization of electro active sol gel/polymer composites. In Proceedings of the 9th International Symposium on Electrets (ISE 9) Proceedings, Shanghai, China, 27 September 1996
[35] Wu, K., Cheng C., Interface charges between insulating materials. IEEE Trans. Dielectr. Electr. Insul., 24, (2017) 2633.
[36] Tsangaris G. M., Koulombi N., Kyvelidis S., Interfacial Relaxation Phenomena in Particulate Composites of Epoxy Resin with Copper or Iron Particles. Mater. Chem. Phys., 44 (1996) 245.
[37] Yuan Q., Bateman S. A., Wu D., Mechanical and Conductive Properties of Carbon Black-filled High-density Polyethylene, Low-

density Polyethylene, and Linear Low-density Polyethylene. J. Compos. Mater. 23 (2010) 459.

[38] Mujal-Rosas R., Marín-Genesc, M., García-Amoró, J., Salueña-Berna X., Colom-Fajula X., Influence on the mechanical properties of various polymeric composites reinforced with GTR particles. Afinidad 76 (2019) 76, 588.

[39] Deng H., Lin L., Ji M., Zhang S., Yang M., Fu Q., Progress on the morphological control of conductive network in conductive polymer composites and the use as electroactive multifunctional materials. Prog.Polym. Sci. 39 (2014) 627.

[40] Pan Y., Liu X., Hao X., Starý Z., Schubert D.W., Enhancing the electrical conductivity of carbon black-filled immiscible polymer blends by tuning the morphology. Eur. Pol. J. 78 (2016) 106.

[41] Mott N.F., J. Non-Cryst. Solids 1 (1968) 1.

[42] Billings M. J., Smith A., Wilkins R., Tracking in Polymeric Insulation. IEEE Trans. Electr. Insul. EI-2 (1967) 131.

[43] Li S., Yu S., Feng Y., Progress in and prospects for electrical insulating materials. HighVolt. 1 (2016) 122.

[44] Teyssedre G., Laurent C., Charge Transport Modeling in Insulating Polymers: From Molecular to Macroscopic Scale. IEEE Trans. Dielectr. Electr. Insul. (2005) 12.

[45] Crone B. K., Campbell I. H., Davids P. S., Smith D. L., Device model for single carrier organic diodes. J. Appl. Phys. 82 (1997) 6319.

[46] Jadhav S. R., Khairnar U. P., Archives of Applied Science Research 4 (1) (2012) 169.

[47] Mane R. M., Kharade R. R., Patil N. S., P. N. Bhosale, Archives of Applied Science Research 2(2) (2010) 275.

[48] Nixon G., Vijayakumar S., Rathnakumari M., Sureshkumar P., Archives of Applied Science Research 3(5) (2011) 514.

[49] AL-Mudhaffera M. F., Nattiqb M. A., Jaberb M. A., Archives of Applied Science Research 4(4) (2012) 1731.

[50] Sharma A. K., Ramu Ch. Dielectric properties of solution grown cellulose acetate thin films. Mater Lett 11(3–4)(1991) 128.

[51] Urbach F. The long wavelength edge of photographic sensitivity and electronic absorption of solids. Phys. Rev., 92 (1953) 1324.

[52] Yakuphanoglu F., Ilican S., Caglar M., et al. The determination of the optical band and optical constants of non-crystalline and crystalline ZnO thin films deposited by spray pyrolysis. J. Optoelectron. Adv. Mater. 9(7) (2007) 2180.

[53] Ramadin Y., Ahmad M., Zihlif A., et al. The optical properties of poly(ethylene oxide) polymer dispersed salt complex. J. Thermoplast. Compos. Mater. 13(6)(2000) 451.

[54] Pankove J. I., "Optical Processes in Semiconductors", (Englewood Cliffs, New Jersey, (1971).

[55] Madhuri K. V., Naidu B. S., Hussain O. M., Eddrief M., Julien C., J., Materials Science and Engineering B 86 (2001) 165.